



Airloads on Bluff Bodies, with Application to the Rotor-Induced Downloads on Tilt-Rotor Aircraft

W.J. McCroskey, Ph. Spalart, G.H. Laub, M.D. Maisel
and B. Maskew

(NASA-TM-84401) AIRLOADS ON BLUFF BODIES,
WITH APPLICATION TO THE ROTOR-INDUCED
DOWNLOADS ON TILT-ROTOR AIRCRAFT (NASA)
15 p HC A02/MF A01

N84-11142

CSCL 01A

Unclass

G3/02 42414

September 1983

NASA
National Aeronautics and
Space Administration

United States Army
Aviation Research
and Development
Command



Airloads on Bluff Bodies, with Application to the Rotor-Induced Downloads on Tilt-Rotor Aircraft

W. J. McCroskey, Aeromechanics Laboratory, Research and Technology Laboratories
U. S. Army Aviation Research and Development Command
Ames Research Center, Moffett Field, California

Ph. Spalart, Ames Research Center, Moffett Field, California

G. H. Laub and M. D. Maisel, Aeromechanics Laboratory, Research and Technology Laboratories
U. S. Army Aviation Research and Development Command
Ames Research Center, Moffett Field, California

B. Maskew, Analytical Methods, Inc., Bellevue, Washington



National Aeronautics and
Space Administration

Ames Research Center
Moffett Field, California 94035

United States Army
Aviation Research and
Development Command
St. Louis, Missouri 63166



AIRLOADS ON BLUFF BODIES, WITH APPLICATION TO THE ROTOR-INDUCED
DOWNLOADS ON TILT-ROTOR AIRCRAFT

COPY
OF POC

W. J. McCroskey, Ph. Spalart, G. H. Laub, and M. D. Maisel

NASA and U.S. Army Aeromechanics Laboratory (AVRADCOM)
Ames Research Center, Moffett Field, California

and

B. Maskew

Analytical Methods, Inc., Bellevue, Washington

Abstract

The aerodynamic characteristics of airfoils with several flap configurations have been studied theoretically and experimentally in an environment that simulates a wing immersed in the downwash of a hovering rotor. Special techniques have been developed for correcting and validating the wind-tunnel data for large blockage effects, and the test results have been used to evaluate two modern computational aerodynamics codes. The combined computed and measured results show that improved flap and leading-edge configurations can be designed which will achieve large reductions in the downloads of tilt-rotor aircraft, and thereby improve their hover efficiency.

I. Introduction

The impingement of the wake of a lifting rotor on a horizontal surface, such as a wing, fuselage, or control surface, degrades the lifting capabilities of the aircraft in hover and low-speed flight. This "download" or vertical drag phenomenon, is particularly important for tilt-rotor type configurations, since both the downwash velocities of the rotors and the affected wing area are larger than for conventional helicopters. For example, the estimated download penalty in hover for the XV-15 aircraft (Fig. 1) varies between approximately 5% and 15% of the gross weight of the aircraft, depending on operating conditions and the setting of the wing flaps.



One practical, operational aspect that illustrates the complexity of the three-dimensional, rotational, separated-flow phenomena is contained in Fig. 2.

This figure shows that the minimum download does not occur when the flaps are fully deflected (that is, when the minimum wing area is exposed to the rotor downwash) but rather when the flaps are deflected approximately 60°. As explained in Section VI, this curious behavior now appears to be caused by flow separation on the upper surface

Fig. 1. The XV-15 Tilt-Rotor Aircraft in hovering flight, wing flaps fully deflected.

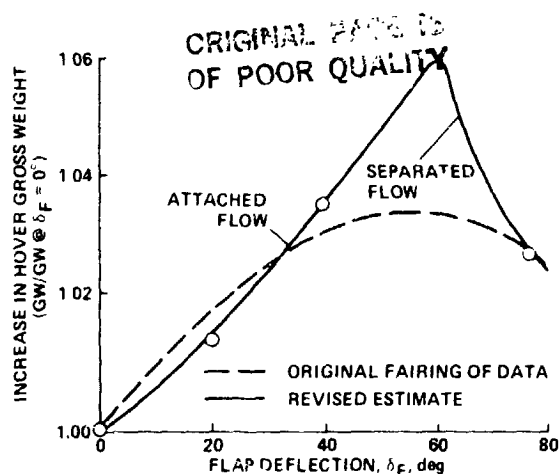


Fig. 2. The effect of flap deflection on hover performance (Ref. [1]).

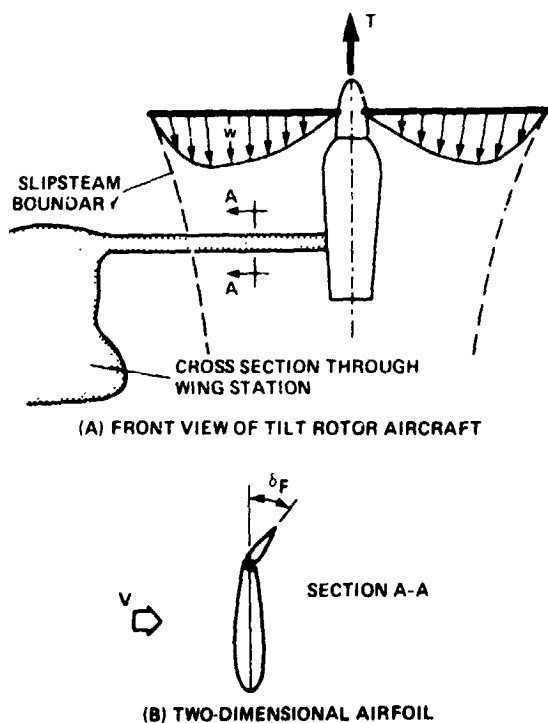


Fig. 3. The rotor download problem and a strip-theory approximation.

number, and the limited number of quantities that are feasible to measure. These limitations are easily overcome by the numerical methods, and in addition, the effort involved in changing the computer input to modify the airfoil shape is much less than that of modifying physical wind-tunnel models. The flexibility to change the geometry at will and to examine the flow-field solutions in detail leads to a better theoretical understanding of the physics of the problem. However, the physical modeling and approximations of the numerical methods have to be examined and verified, and further improvements are required to determine the absolute values of the airloads with confidence. We shall show that while both the experimental

of the flaps and flaperons. However, current engineering prediction techniques give no clue to the mechanism responsible for the results shown in Fig. 2. In fact, they do not even predict the overall effects of the rotor-wing interference adequately, nor do they provide reliable design guidelines for reducing the rotor-induced downloads.

A logical first step in developing new phenomenological information and predictive capability for this class of rotor-body interference aerodynamics would be to study the two-dimensional section characteristics of a wing in the wake of a rotor, or even more simply, to study an airfoil placed normal to an oncoming uniform flow (Fig. 3). This novel configuration is the basis of the present combined theoretical and experimental investigation. A special wind tunnel experiment has been performed for this problem, and two new modern computational aerodynamics methods have been explored to complement the measurements. The resultant two-dimensional data are expected to approximate the section characteristics that are being measured in a separate investigation at various spanwise stations of the actual XV-15 Tilt Rotor Aircraft in hovering flight.

An important aspect of the present investigation is the combination of experimental information and computational analysis. The experiment provides some definitive facts about the real separated viscous flow, but it has specific limitations with respect to wind-tunnel wall corrections, Reynolds

and numerical approaches have definite shortcomings, the proper combination of computations and measurements gives more information than can be derived from either method alone.

II. Experimental Investigation

Two-dimensional models of the XV-15 wing with various flap and leading-edge configurations were tested between endplates in the U.S. Army Aeromechanics Laboratory 2 x 3 meter subsonic wind tunnel. Figure 4 shows the wing sections that were used to obtain the results given in this paper. The airfoil shown (a modified NACA 64A223 profile with a 25% plain flap) represents the XV-15 aircraft; 30% and 35% trailing-edge flaps were also tested. The trailing-edge flaps were deflected in 15° increments up to 90°. The modified leading edge was designed on the basis of preliminary calculations which revealed that the drag characteristics are highly sensitive to the surface curvature distributions in certain critical regions on the upper, or "windward," side of the airfoil.

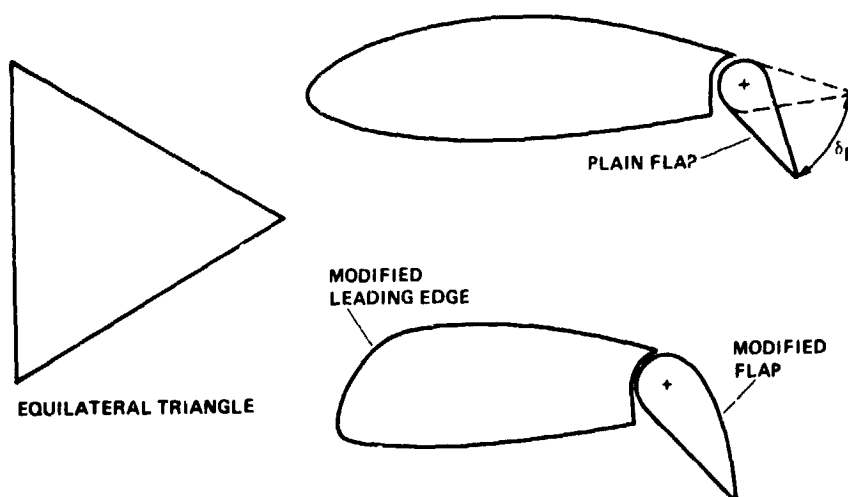


Fig. 4. Sketch of the models tested.

The chord of the basic model (with $\delta_F = 0$ and no leading-edge modifications) was 0.31 m. This represented a difficult compromise between the requirements to maximize Reynolds numbers, minimize wind-tunnel blockage and wall effects, and minimize three-dimensional effects. The Reynolds number for the airfoil results presented herein was 10^6 . The results for a number of additional configurations and for ranges of angles of attack and Reynolds numbers are given in Ref. [2], along with further details of the experimental setup.

In addition to the airfoils, two wedge-shaped models having equilateral-triangle cross sections, with $c = 0.22$ and 0.31 m, were tested with the apex pointed both forward and rearward. These two orientations produced values of C_D that were comparable to or greater than the values for the various flap settings. The data from these models were essential in developing and validating the test techniques, as explained in Section IV. The Reynolds number based on c varied from 0.4 to 1.3×10^6 for the triangles.

A typical model installation is shown in Fig. 5. The spar of the models was cantilevered from the frame of a force-and-moment balance beneath the floor of the test section. A turntable in the balance frame allowed the model angle of attack to be adjusted $\pm 20^\circ$ from perpendicular to the free stream. Large endplates, based on the observations and recommendations of Ref. [3], were installed 0.31 m from the wind-tunnel floor and ceiling to minimize the interaction between the tunnel-wall boundary layer and the wake of the model. The small gaps between the ends of the models and the endplates were not sealed.

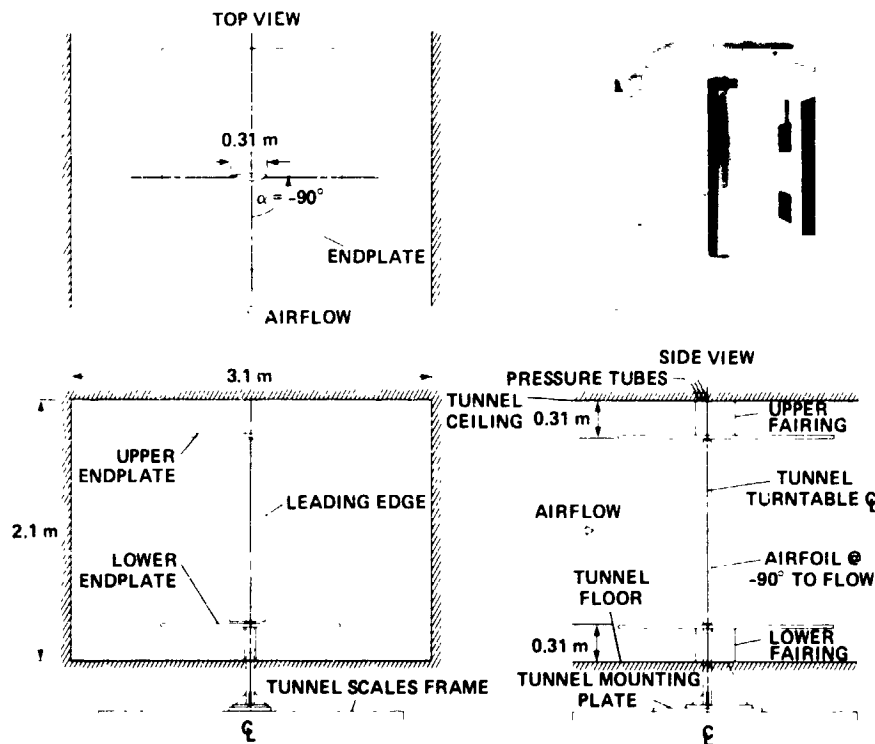


Fig. 5. Wind-tunnel installation.

The average aerodynamic forces were derived from the wind-tunnel balance system and static pressure distributions were measured at three spanwise locations on the airfoils. For the triangles, only two static pressure taps were installed on each face at each of the three spanwise locations. Other measurements included oil flow and wool tuft visualizations of the separation patterns and wake surveys with fast-response pressure transducers.

These flow visualization studies and spanwise traverses, along with the measured spanwise pressure distributions, indicated that the flow was uniform in the vertical direction to within the accuracy of the measurements even though the aspect ratios of the large triangle and the airfoil models were only 5. Furthermore, no evidence was found of spanwise cells in the wake structure. The rather large blockage ratio (up to 10% based on the frontal area between the endplates) was a matter of concern and special study, but as indicated in Section IV, the corrected data for the triangles agreed well with previously published results.

III. Numerical Methods of Analysis

ORIGINAL PAGE IS
OF POOR QUALITY

The first aerodynamic code to be considered was developed by the second author (Refs. [4,5]) to calculate the separated flow, wake, and fluctuating airloads on two-dimensional bluff bodies or airfoils at arbitrary angles of attack and at high Reynolds number. This technique combines an integral boundary layer with a discrete vortex method for the outer flow. The two-dimensional vorticity-conservation equation is solved in a Lagrangian formulation, wherein the vorticity field is represented as the sum of local patches, or "blobs," of vorticity which retain their strength in time and are convected by the flow. The vortices are introduced along the walls of the body at each time step, and their positions at subsequent time steps are determined numerically using the Adams-Bashforth-2 multistep time-integration scheme. The resultant velocity field computed by the Biot-Savart law is used in a boundary-layer calculation to determine the separation point. Viscous diffusion is neglected outside the attached boundary layer and no empiricism is introduced.

The present discrete-vortex method does not use conformal mapping; hence, it can treat arbitrary shapes and multiple bodies. This feature has been exploited to include flat surfaces that represent wind-tunnel walls, which is essential for quantitative comparison with the experiment. The code gives the complete time-dependent development of the entire flow field, including vortex shedding. However, it requires relatively large computational resources for large numbers of vortices; a typical case requires 10-15 min CPU time on the Ames Cray 1S computer. Figure 6 shows a typical result. Here the dots are the individual vortices and the contour lines are the instantaneous streamlines.

The second code is a recent adaptation by the fifth author of the program VSAERO (Ref. [6]), which combines an efficient three-dimensional, unsteady potential-flow panel method with a free-streamline representation of the separated zone. Planar quadrilateral panels are used to represent the body and wake surfaces. Each panel has a constant source and doublet distribution and a central control point where an internal Dirichlet boundary condition is applied. Large regions of separated flow are modeled in the manner of the CLMAX program (Ref. [7]), which assumes an inviscid wake with total pressure that is less than the free stream value. The separated-wake region is enclosed by a pair of constant-strength vortex sheets.

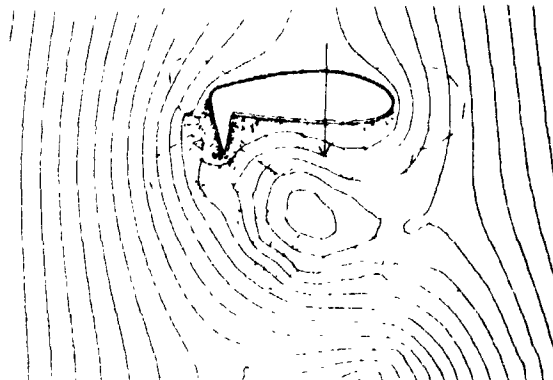


Fig. 6. The instantaneous flow field computed around an NACA 4421 airfoil. The arrow indicates the position, magnitude, and direction of the resultant force vector.

The calculations for this method proceed as follows: an initial solution is assumed, including the separation points and the shape of the wake, and then the solution is stepped forward in time. The dividing streamlines between the potential-flow zones and the wake region are transported with the local outer flow at each time step using the calculated velocities of points on the wake surfaces, thereby satisfying the condition that the wake vortex sheets be force-free. In the present case, no attempt

is made to model the unsteady vortex shedding phenomenon; rather, the code is run until the solution converges to a steady-state solution that approximates the time-averaged separated flow around the body, usually within 10 time steps.

By its nature, this code contains more approximations and empiricism than the discrete-vortex approach. However, the two-dimensional version requires only about 100 sec of

CPU time per case on a Prime 550 computer to converge to a steady solution; this would be equivalent to one or two seconds on the Cray 1S. Figure 7 shows a typical result. The large suction peak on the upper surface at $x/c \approx 0.85$ is due to the rapid expansion around the shoulder of the flap.

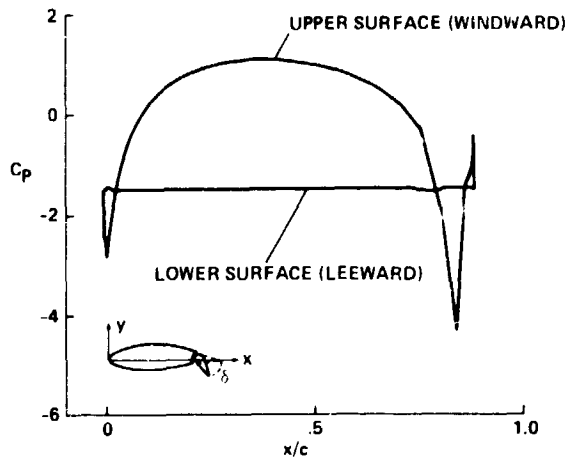


Fig. 7. Pressure distribution on the NACA 64A223-M airfoil at $\alpha = -90^\circ$ and $\delta_F = 60^\circ$.

Both of the codes used in this study have been adapted to include airfoils with flaps, multiple-element airfoils, and exterior boundaries such as wind-tunnel walls. This latter capability is essential for detailed comparison with the experiment and for verifying the wall corrections that were applied to the data.

IV. Results and Discussion - Triangles

A. Validation of the Experiment, Including Blockage Corrections

When a model is tested in a closed-section wind tunnel, it creates a blockage that accelerates the local flow and increases the drag. These effects are known to be proportional to the drag and the physical size of the model. For two-dimensional tests, Allen and Vincent (Ref. [8]), Pankhurst and Holder (Ref. [9]), and Maskell (Ref. [10]) give theoretical blockage corrections that take the following form for bluff bodies.

$$\frac{C_D}{C_{D_0}} \approx 1 - \epsilon b C_{D_0} \quad (1)$$

$$\frac{C_p - 1}{C_{p_0} - 1} = \frac{C_D}{C_{D_0}} \quad (2)$$


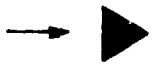


where ϵ is a constant, b is the ratio of the lateral dimension of the model to the lateral dimension of the wind tunnel, C_D is the two-dimensional drag coefficient in free air, and C_{D_0} is the measured uncorrected value of the drag coefficient. Also, C_p and C_{p_0} are the corrected and uncorrected values of the pressure coefficient, respectively.

References [8-10] give theoretical values of ϵ ranging from 0.50 to 0.96, and numerous previous wind-tunnel measurements on cylinders of various cross sections suggest values between these limits. Further support for this approach was obtained from the present discrete-vortex computational method. The results for airfoils at $\alpha = -90^\circ$ between solid walls were found to correlate well with Eq. 1 for blockage ratios in the range $0 \leq b \leq 0.20$, giving $\epsilon = 0.65 \pm 0.05$.

Therefore, the form of Eq. 1 seems to be appropriate here, provided a reasonable estimate of ϵ can be obtained. This empirical constant was obtained from the present data for the two different sizes of triangles tested at the two different orientations, giving four combinations of the product bC_{D_0} . The corresponding free-air drag coefficients have been well documented in Ref. [11]; $C_D = 2.00$ for the blunt face forward and $C_D = 1.30$ for the apex forward. The measured values for 15 combinations of Reynolds numbers, sizes, and orientations then yielded $\epsilon = 0.596$, with a standard deviation of only ± 0.024 . As this value is in good agreement with the various independent studies cited above, it was used to correct the airfoil data described in the following section.

The experimental results for the triangles are summarized in Table 1. Only the average values of the various experimental quantities are listed, as they were found to be independent of Reynolds number, to within the experimental uncertainty. All of the results are in excellent agreement with Hoerner (Ref. [11]), with the exception that the Strouhal frequency for the triangles with the apex forward ($St = fb/U_\infty$) does not correlate with his empirical formula using C_D . It is interesting to note that the corrected base pressure coefficient, C_{p_b} , is essentially independent of the orientation of the triangle, even though C_D and St are not.

TABLE 1. SUMMARY OF RESULTS FOR THE EQUILATERAL TRIANGLES

Configuration	C_{D_0}	C_D	C_D (Ref. 11)	$C_{p_{base}}$	$C_{p_{base}}$ (Ref. 11)	St	St (Ref. 11)
	2.31	1.99	2.00 1.98 ¹	-1.17	-1.13 ¹	0.128	0.123 ²
	2.25	2.03	2.00 1.98 ¹	-1.24	-1.13 ¹	0.123	0.123 ²
	1.41	1.29	1.30	-1.12	-1.13 ¹	0.200	0.173 ²
	1.38	1.30	1.30	-1.18	-1.13 ¹	0.204	0.173 ²

¹Flat plate normal to flow.

²Hoerner: $St = 0.21 C_D^{-3/4}$.

ORIGINAL PAGE IS
OF POOR QUALITY

B. Validation of the Computational Methods

The data in Table 1 can now be used to evaluate the present computational methods. Figure 8 shows the free-air drag coefficient for triangles as a function of the semi-vertex angle. As seen from the figure, the simpler panel method gives reasonably good results, but the vortex method does not. On the other hand, the computed Strouhal shedding frequencies of the vortex shedding (not shown) were within a few percent of the experimental values. The main difficulty with the vortex method seems to be that the computed base pressure is much too large, $C_{pb} \approx -2.0$ vs -1.2 in the experiment, and this is responsible for the excessive values of C_D . The panel method gives approximately the correct base pressure for both of the triangles tested.

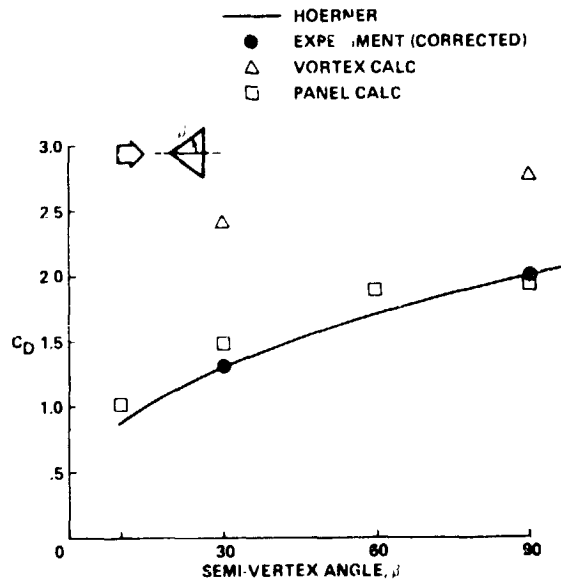


Fig. 8. Drag coefficients for triangles as a function of semivertex angle.

Despite efforts to determine the deficiency in the vortex method, the reasons for it remain unknown. The method was shown in Refs. [4] and [5] to predict dynamic stall on an oscillating airfoil and the flow field of a circular cylinder reasonably well, but was less successful in determining the drag of a square cylinder, which was found to be too low. A sensitivity study of the numerical parameters such as time step, number of points used to define the body, number of vortices, and vortex core radius has thus far failed to reveal any clear trends.

However, it should be mentioned that previous investigators of vortex methods have found it necessary to reduce empirically the circulation of the vortices after they leave the body (cf. Sarpkaya [12]). This is often argued as modeling vorticity dissipation due to viscosity even though vorticity only diffuses within the framework of the Navier-Stokes equations. To test the importance of diffusion, the effects of viscosity were simulated in test calculations by means of Chorin's "random walk" (Ref. [13]). Changes in the base pressure were found; but only by simulating low values of Reynolds number on the order of 100, was the drag reduced to approximately the experimental values. The remaining possibility is that the vorticity in the wake becomes highly three-dimensional and this may somehow reduce its effective induced-velocity field in the plane of the mean flow. At present, however, the present vortex method cannot be considered reliable for quantitative predictions without empiricism, although it may be valuable for predicting trends.

V. Results and Discussion - Airfoils

The primary objectives of this investigation were to determine the aerodynamic characteristics of the XV-15 airfoil section with various flap

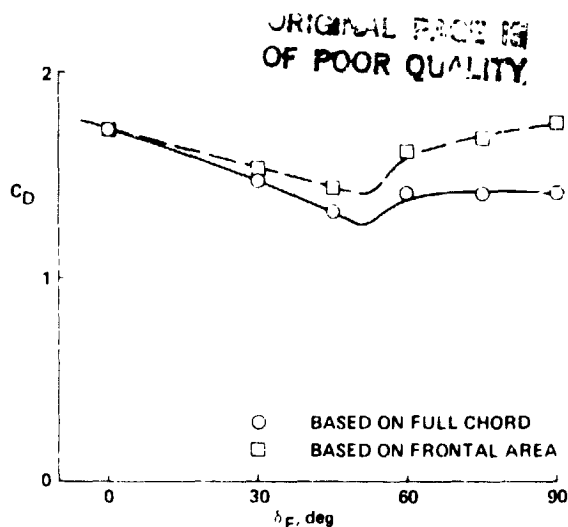


Fig. 9. Measured drag coefficients of the airfoil with 25% trailing-edge flap as a function of flap deflection angle.

The results show that for flap deflection angles less than 60° , the total drag decreases significantly more than could be explained on the basis of the reduction in frontal area. However, for $\delta_F > 60^\circ$, the total drag remains approximately constant, and C_D based on frontal area actually increases. Tuft and oil-flow visualization revealed this to be a result of flow separation occurring on the flap just downstream of the shoulder of the flap and ahead of the trailing edge. This produced a wider wake behind the airfoil, less suction on the front face of the airfoil, a somewhat lower base pressure, and higher drag.

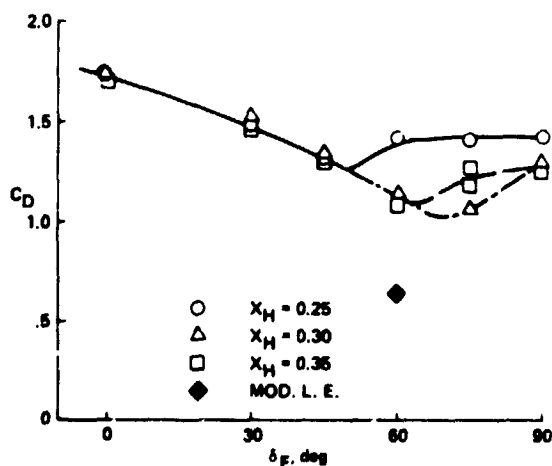


Fig. 10. Measured drag coefficients for several airfoil configurations: C_D is based on the chord of the airfoil with $\delta_F = 0$, x_H is the location of the flap hinge axis.

deflections and to determine whether the tilt-rotor downloads could be reduced by improved airfoil and flap designs. Figure 9 shows the measured results for the drag coefficient for the XV-15 profile. These results are based on two different reference areas: (1) the area of the basic airfoil with no flap deflection, and (2) the actual projected frontal area. In the latter case, the purely geometrical effect of reducing the surface area normal to the flow has been eliminated, and the variation in drag coefficient defined in this way is due to the modified aerodynamics alone. The shapes of the faired curves between $\delta_F = 45^\circ$ and 60° were determined from crossplots of the results at other angles of attack.

Figure 10 shows a comparison of the experimental results for all three flap sizes and for the modified leading edge, as depicted in Fig. 4. The larger flaps supported attached flows to larger flap-deflection angles, with correspondingly lower values of C_D . A minimum value of $C_D = 1.0$ is estimated for the unmodified leading edge. However, the modified leading-edge reduced the minimum drag coefficient to only 0.64 with $\delta_F = 60^\circ$. These results indicate the potential value of wing modifications in reducing the downloads on the tilt-rotor aircraft.

Figures 11 and 12 show the computations for the airfoil with a 25% trailing-edge flap in comparison with the measured data from Fig. 9.

It is clear from Fig. 11 that the quantitative predictions leave something to be desired, especially regarding the results of the vortex method. However, Fig. 12 indicates that the trends can be predicted quite well; for the drag coefficient ratio, the

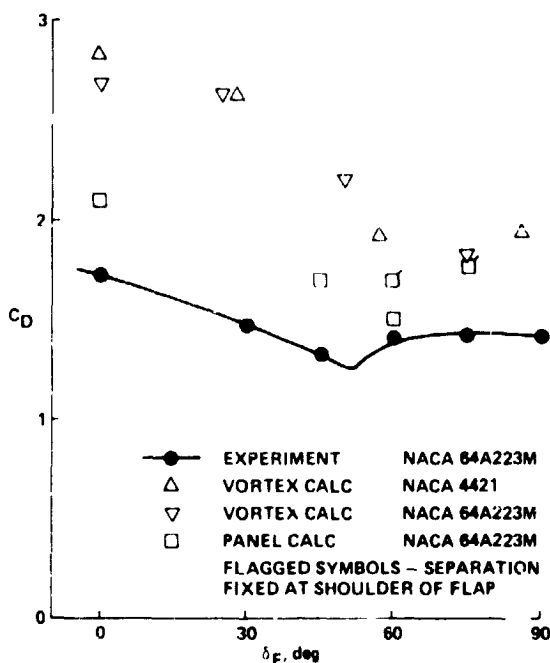


Fig. 11. Comparison of measured and calculated drag coefficient as function of flap deflection angle.

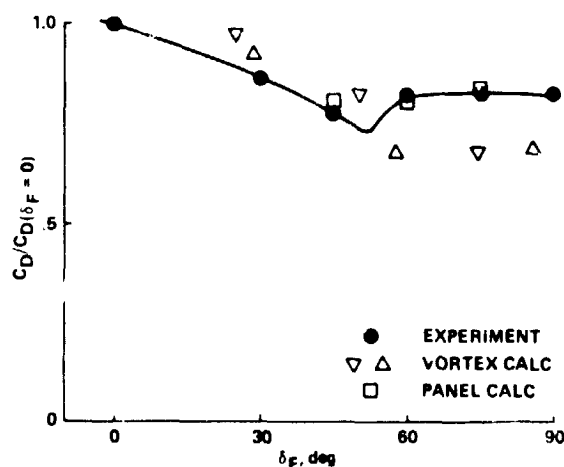


Fig. 12. Measured and calculated drag coefficients normalized by the values for $\delta_F = 0$.

panel method agrees with the measurements to within experimental accuracy. It is also interesting to note the following ratios of C_D for the airfoil with the modified leading edge and $\delta_F = 60^\circ$ compared to the basic airfoil with $\delta_F = 0$: experiment, 0.37; vortex method, 0.53; panel method, 0.49.

Figure 13 shows a comparison of the measured pressure distribution vs that predicted by the panel method. In its present preliminary form, the unsteady panel code does not include a boundary-layer calculation and the separation point must be prescribed. However, it is clear from the pressure distributions that the flow would not remain attached all the way to the

trailing edge in this case; therefore, fixing the separation point on the shoulder of the flap gives somewhat better results. As the location of the separation point is likely to be less obvious in other cases, the logical next step in the development of the method is to include a boundary-layer model.

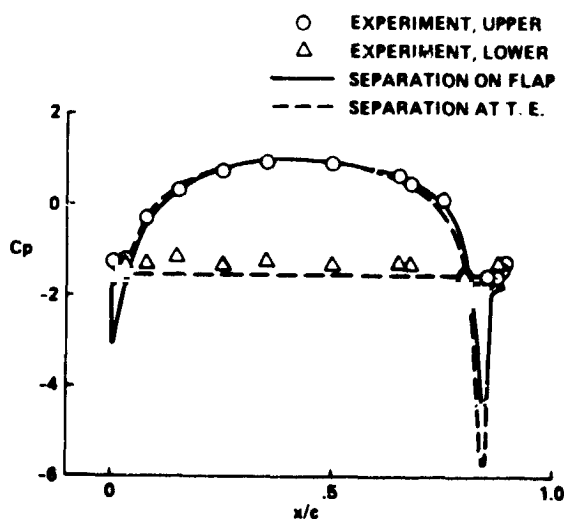


Fig. 13. Measured and predicted pressure distributions for $\delta_F = 60^\circ$.

VI. Concluding Remarks

This investigation has produced new insight and quantitative information about the airloads on bluff bodies, with particular relevance to the complicated aerodynamic interference between the rotors and the wing of tilt-rotor aircraft configurations. Both the calculations and the experiment show that the drag of an airfoil normal to the oncoming flow decreases as the flap deflection angle increases, up to the point where the flow begins to separate on the flap. Furthermore, the reduction in drag is considerably more than would be due merely to the reduction in the projected area normal to the flow. However, the drag increases with increasing δ_F once separation appears on the flap, and this occurs well before the upper surface of the flap is aligned parallel with the free-stream flow.

The results for the airfoil model of the XV-15 wing (Fig. 9) help to explain the behavior of the flight-test data in Fig. 2, as discussed in the Introduction. The hover performance is, of course, directly affected by the download on the wing (that is, by C_D), which depends strongly upon δ_F . Therefore, it is clear that the gross-weight capability in hover should increase with increasing flap deflection until flow separation begins to occur on the flaps, but that excessive flap deflections would increase the wing download and decrease the maximum gross weight in hover. The dashed line in Fig. 2 is the original fairing of the data as presented in Ref. [1], whereas the solid line represents the revised estimate based on the results of the present investigation.

The combined results of this investigation also indicate that significant further improvements in hover efficiency could be attained by careful design of the wing sections. The most obvious possibilities include the use of larger flaps, flaps with larger radii of curvature at the shoulder, and appropriate changes in the curvature distribution in the leading-edge region of the wing. Multielement airfoils were not considered in this paper, but some further drag reductions due to extra devices are described in Ref. [2].

The experimental techniques that were developed with the aid of the computational methods and the triangle models appear to have been very successful in dealing with and correcting for the relatively large blockage ratios of the airfoils. As a side benefit, some additional data have been added to what exist in the general literature for arbitrary bluff bodies. The quantitative accuracy of the discrete-vortex computational method turned out rather disappointing, although it was still useful. The reasons for its failure and a means of introducing suitable empiricism should be examined further. On the other hand, the panel method with the free-streamline representation of the separated wake is quite promising. As mentioned in Section V, some means of estimating the separation points by boundary-layer theory is essential if the method is to be used to design the optimum curvature distributions in the leading-edge region and near the shoulder of the flap. Further refinements are needed to enhance its quantitative accuracy as well, but the method seems to be a good, inexpensive engineering tool to study complex flow problems.

Finally, it should be emphasized that the present investigation was concerned entirely with a two-dimensional approximation to a very complicated three-dimensional aerodynamic-interference problem. The results indicate that considerable improvements are possible and practical in the area of rotor-induced downloads, but similar studies for realistic

rotor-wing combinations will be essential to help the tilt-rotor concept achieve its full potential.

References

- 1) M. Maisel and D. Harris, Hover Tests of the XV-15 Tilt Rotor Research Aircraft, AIAA Paper 81-2501, 1981.
- 2) M. Maisel, G. Laub, and W. L. McCroskey, Wind Tunnel Investigations of Two-Dimensional Wing Configurations at Inflow Angles near -90, NASA TM, in preparation.
- 3) P. K. Stansby, The Effects of End Plates on the Base Pressure of a Circular Cylinder, Aeronautical Journal, Vol. 78, No. 1, pp. 36-37, 1974.
- 4) P. Spalart and A. Leonard, Computations of Separated Flows by a Vortex Tracing Algorithm, AIAA Paper 81-1246, 1981.
- 5) P. R. Spalart, A. Leonard, and D. Baganoff, Numerical Simulation of Separated Flows, NASA TM-84238, 1983.
- 6) B. Maskew, Predictions of Subsonic Aerodynamic Characteristics - A Case for Low-Order Panel Methods, AIAA Paper 81-0252, Jan. 1981.
- 7) B. Maskew and F. A. Dvorak, The Prediction of C_{l-max} Using a Separated Flow Model, J. Am. Hel. Soc., Vol. 23, No. 2, pp. 2-8, Apr. 1978.
- 8) H. J. Allen and W. G. Vincenti, Wall Interference in a Two Dimensional Flow Wind Tunnel, with Consideration of the Effect of Compressibility, NACA Report 782, 1944.
- 9) R. C. Pankhurst and D. W. Holder, Wind Tunnel Techniques, Pitman, 1952.
- 10) E. C. Maskell, A Theory of the Blockage Effects on Bluff Bodies and Stalled Wings in a Closed Wind Tunnel, Aero. Res. Coun. R&M 3400, 1963.
- 11) S. F. Hoerner, Fluid Dynamic Drag, published by the author (Dr.-Ing. S. F. Hoerner, 148 Busteed Drive, Midland Park, New Jersey 07432), 1965.
- 12) T. Sarpkaya, Vortex-Induced Oscillations - a Selective Review, ASME J. Applied Mech., Vol. 46, No. , pp. 241-258, 1979.
- 13) A. J. Chorin, Numerical Study of Slightly Viscous Flow, J. Fluid Mech., Vol. 57, Part 4, pp. 785-796, 1973.